



HAL
open science

The equation of state of TaC_{0.99} by X-ray diffraction in radial scattering geometry to 32 GPa and 1073 K

Sergio Speziale, Julia Immoor, A Ermakov, Sébastien Merkel, Hauke Marquardt, Hanns-Peter Liermann

► To cite this version:

Sergio Speziale, Julia Immoor, A Ermakov, Sébastien Merkel, Hauke Marquardt, et al.. The equation of state of TaC_{0.99} by X-ray diffraction in radial scattering geometry to 32 GPa and 1073 K. *Journal of Applied Physics*, 2019, 126 (10), pp.105107. 10.1063/1.5115350 . hal-02284714

HAL Id: hal-02284714

<https://hal.univ-lille.fr/hal-02284714v1>

Submitted on 12 Sep 2019

HAL is a multi-disciplinary open access archive for the deposit and dissemination of scientific research documents, whether they are published or not. The documents may come from teaching and research institutions in France or abroad, or from public or private research centers.

L'archive ouverte pluridisciplinaire **HAL**, est destinée au dépôt et à la diffusion de documents scientifiques de niveau recherche, publiés ou non, émanant des établissements d'enseignement et de recherche français ou étrangers, des laboratoires publics ou privés.

This is the author's peer reviewed, accepted manuscript. However, the online version of record will be different from this version once it has been copyedited and typeset.
PLEASE CITE THIS ARTICLE AS DOI: 10.1063/1.5115350

1 The equation of state of TaC_{0.99} by X-ray diffraction in radial scattering geometry to 32
2 GPa and 1073 K

3 S. Speziale^{1,*}, J. Immoor², A. Ermakov³, S. Merkel⁴, H. Marquardt^{2,5}, H.P. Liermann³

4 ¹German Research Centre for Geosciences GFZ, Telegrafenberg, D-14473 Potsdam,
5 Germany

6 ²Bayerisches Geoinstitut (BGI), University of Bayreuth, 95440 Bayreuth, Germany

7 ³Photon Sciences, Deutsches Elektronen Synchrotron (DESY), FS-PE Building 47c,
8 22607 Hamburg, Germany

9 ⁴Unité Matériaux Et Transformations (UMET), University of Lille, Bâtiment C6, 59655
10 Villeneuve d'Ascq, France

11 ⁵Department of Earth Sciences, University of Oxford, South Parks Road, Oxford OX1
12 3AN, U.K.

13 *Corresponding author email: speziale@gfz-potsdam.de

14 **Abstract.** We have performed in situ synchrotron X-ray diffraction experiments on
15 TaC_{0.99} compressed in a diamond anvil cell along 3 isothermal paths to maximum
16 pressure (P) - temperature (T) conditions of 38.8 GPa at 1073 K. By combining
17 measurements performed in axial diffraction geometry at 296 K and in radial geometry at
18 673 K and 1073 K, we place constraints on the pressure-volume-temperature (P-V-T)
19 equation of state of TaC in a wide range of conditions. A fit of the Birch-Murnaghan
20 equation to the measurements performed in axial geometry at ambient temperature yields
21 a value of the isothermal bulk modulus at ambient conditions $K_{T0} = 305 \pm 5$ (1 σ) GPa
22 and its pressure derivative $(\partial K_T / \partial P)_{T0} = 6.1 \pm 0.5$. The fit of the Birch-Murnaghan-

23 Debye model to our complete P-V-T dataset allows us to constrain the Grüneisen
24 parameter at ambient pressure $\gamma_0 = V(\partial P/\partial E)_{V_0}$ to the value of 1.2 ± 0.1 .

25

26 **I. INTRODUCTION**

27 Tantalum carbide TaC_x ($0.6 < x < 1$) is a B1 structured ultra-high temperature ceramic
28 (UHTC) [1]. UHTC materials have the potential to be used in different technological
29 applications because of their combined high mechanical strength, extremely good thermal
30 stability as well as its resistance to harsh chemical environments.

31 Transition metal carbides are in general among the ceramic materials with the best
32 characteristics for high temperature applications where enhanced refractory and
33 mechanical properties are required [2]. Tantalum carbide has an extremely high melting
34 temperature, low electrical conductivity and unusual mechanical behavior with respect to
35 the other B1 structured (space group $Fm\bar{3}m$) monocarbides of the group IV and V
36 transition metals (TMC) [3, 4].

37 The structural, thermodynamic and transport properties of TaC_x (in the following we will
38 use TaC except when discussing the effect of non-stoichiometry on specific physical
39 properties) have been the subject of many experimental and computational investigations
40 and part of the existing results are tabulated in several review publications together with
41 the properties of the other TMC [5-27]. In particular, the elastic properties of TaC have
42 been the subject of more than ten different experimental and computational studies [6, 15,
43 16, 28-39] exploring the effect of pressure or temperature and non-stoichiometry on the
44 tensor and the aggregate elastic moduli of single crystals or polycrystals.

This is the author's peer reviewed, accepted manuscript. However, the online version of record will be different from this version once it has been copyedited and typeset.
PLEASE CITE THIS ARTICLE AS DOI: 10.1063/1.5115350

45 While several computational studies provide models of the isothermal compression
46 behavior of TaC, only two experimental diamond-anvil cell studies investigate its
47 compression behavior to the multi-GPa stress range at ambient temperature [32, 37]. The
48 first study focuses on the response of micron-sized polycrystalline TaC_{0.98} to compression
49 under different stress conditions, and the second explores the behavior of nanocrystalline
50 TaC under strongly nonhydrostatic stress.

51 To date there are no data on the combined effect of high-pressures, stress and -
52 temperatures on the structure and the thermoelastic properties of tantalum carbide. With
53 this study we give a first account of the compression behavior of TaC_{0.99} compressed to
54 more than 40 GPa at ambient temperature and to a maximum of 38.8 GPa at 1073 K, and
55 we place quantitative constraints on the pressure-volume-temperature (PVT) equation of
56 state of this material.

57 Here we use a new approach to place quantitative constraints on the thermoelastic
58 properties of TaC_{0.99}. We combine the results of static compression experiments in a
59 graphite resistive heated diamond-anvil cell using in situ synchrotron X-ray diffraction in
60 radial scattering geometry (an established technique [40-46] yet never used before in
61 studies dedicated to constrain the pressure-volume-temperature equation of state) with
62 those from axial geometry at room temperatures. The use of high-temperature high-
63 pressure radial diffraction geometry in combination with a theory of non-hydrostatic
64 lattice strains allows us to quantitatively constrain the departure from hydrostatic stress
65 conditions, which is not straightforward in experiments performed in axial geometry.
66 This is particularly relevant for stiff samples such as TaC when they bridge between the
67 culets of the two diamond anvils under combined high pressure and high temperature. In

68 addition the experimental approach used here allows us to measure high temperature
69 volume compression along strictly isothermal compression paths at moderately high
70 temperatures, which is difficult with laser-heated diamond anvil-cell experiments, thus
71 producing the best suited dataset for P-V-T equation of state fitting.

72

73 **II. MATERIALS AND METHODS**

74 **A. Sample material**

75 The starting material for all experiments presented here is a powder of TaC_{0.99} (with
76 nominal stoichiometric TaC composition) produced by American Elements©. We have
77 determined the chemical composition of our starting material by measuring its unit-cell
78 volume by X-ray diffraction at the German Research Centre for Geosciences (GFZ) using
79 a STOE Stadi P diffractometer with Cu K α radiation monochromatized by a Ge(111)
80 crystal. Two separate amounts of sample were mixed with ~10 wt% Si standard (NIST
81 640d) as an internal calibrant. The average of the two measurements yields a unit-cell
82 parameter $a_0 = 4.4555 \pm 0.0007$ Å. This value corresponds to a composition of TaC_{0.99}
83 based on the calibration by Bowman [8]. The unit cell parameter of our sample is
84 equivalent within uncertainty to the results of neutron diffraction measurements of a
85 disordered stoichiometric TaC [9] and 3σ larger (rather than smaller, as expected) than a
86 more recent neutron diffraction study of nominally stoichiometric TaC [10].

87

88 **B. High-pressure synchrotron X-ray diffraction in axial geometry**

89 In these experiments the axis of the diamond anvils is parallel to the incident X-ray beam.

This is the author's peer reviewed, accepted manuscript. However, the online version of record will be different from this version once it has been copyedited and typeset.
PLEASE CITE THIS ARTICLE AS DOI: 10.1063/1.5115350

90 TaC_{0.99} was compressed quasi-hydrostatically in a symmetric piston-cylinder type
91 diamond anvil cell [47] with 300 μm culet diamonds. Fine sample powder (with less than
92 1 μm average grain-size) was loaded in a 150 μm wide cylindrical chamber drilled in a
93 250 μm thick rhenium disk pre-indented to a thickness of 30 μm . Neon gas was loaded as
94 a pressure transmitting medium using the gas-loading facility from Core Labs located at
95 PETRA III and operated by the Extreme Condition Science Infrastructure. A ruby sphere
96 and a ~ 5 μm speckle of gently packed gold powder were used as internal pressure
97 standards [48, 49]. The diamond anvil cell was compressed remotely with a gas-
98 membrane system. X-ray diffraction images were collected at the general purpose
99 experiment table of Extreme Conditions Beamline (ECB, P02.2) of the 3rd generation
100 light source PETRA III at DESY, Hamburg, Germany. The monochromatic incident X-
101 ray radiation had a wavelength of 0.2966 \AA . The beam was focused to a spot size of 3 μm
102 (vertical) by 8 μm (horizontal) full width at half maximum by means of Compound
103 Refractive Lenses (CRL). X-ray diffraction images were collected with a Perkin Elmer
104 XRD1621 flat panel detector at 420 mm distance from the sample. The sample to
105 detector distance and tilting angles of the detector were calibrated using a CeO₂ standard
106 from the National Institute of Standards and Technology (NIST, 674b). Twenty X-ray
107 diffraction images were collected at pressures between 5.1 GPa and 43.6 GPa, including
108 3 images collected during decompression. The exposure time for each image was 20 s.
109 The images were analyzed with the Fit2d software package [50]. Le Bail fit [51] of the
110 integrated spectra were performed with the software MAUD [52] to determine the unit
111 cell parameter a (TaC crystallizes in the cubic system in the space group $Fm\bar{3}m$). A
112 typical X-ray diffraction image and the result of the Le Bail fit are shown in Figure 1.

This is the author's peer reviewed, accepted manuscript. However, the online version of record will be different from this version once it has been copyedited and typeset.
PLEASE CITE THIS ARTICLE AS DOI: 10.1063/1.5115350

113 The conditions and the results of the room temperature compression experiments are
114 reported in Tables I and II.

115

116 C. Simultaneous high-pressure high-temperature synchrotron X-ray diffraction in radial
117 scattering geometry

118 Two series of measurements were performed in radial scattering geometry at the general
119 purpose experiment table of the ECB. In these experiments the axis of the diamond anvils
120 is perpendicular to the incident X-ray beam, passing through an X-ray transparent sample
121 chamber, made of a mixture of amorphous boron and epoxy.

122 The setup for these experiments is based on a modified Mao-Bell piston-cylinder type
123 diamond anvil cell equipped with a graphite resistive sandwich heater for high-
124 temperature experiments [53]. Pressure in the diamond anvil cell is controlled remotely
125 by a gas membrane system. For temperature measurements two type-R thermocouples are
126 placed in contact with the diamond at short distance from the culets. The diamond anvil
127 cell is placed in a vacuum vessel (capable of maintaining 10^{-4} mbar pressure during the
128 experiments) to protect diamonds, the metallic parts of the diamond anvil cell and heater
129 setup from oxidation [54].

130 TaC_{0.99} powder with a grain size $< 1 \mu\text{m}$ was loaded in $50 \mu\text{m}$ diameter cylindrical
131 chambers laser-drilled in amorphous boron – epoxy gaskets of $380 \mu\text{m}$ diameter and 50
132 μm thickness. With such a narrow sample-chamber the entire sample remains as close as
133 possible to the center of the diamond culets, where stress gradients are low and where
134 stress and strain fields are close to ideal axial symmetry that is required in the
135 interpretation of X-ray diffraction experiments in radial scattering geometry (see section

This is the author's peer reviewed, accepted manuscript. However, the online version of record will be different from this version once it has been copyedited and typeset.
PLEASE CITE THIS ARTICLE AS DOI: 10.1063/1.5115350

136 II.D). The ceramic gaskets are supported by a kapton ring. In all the experiments the
137 diameter of the diamond culets was 300 μm and no pressure transmitting medium was
138 employed.

139 In the two high-temperature experimental runs a 5-10 μm wide fragment of less than 5
140 μm thick Au foil was placed above the sample as a pressure calibrant. The two high-
141 temperature experimental runs were performed using a monochromatic X-ray beam of
142 0.4847 \AA wavelength with an identical focus spot-size as for the axial diffraction
143 experiment but slightly different sample to detector distance of 405 mm based on the
144 same calibration approach as for the axial diffraction experiment.

145 The exposure time for all images in the radial X-ray diffraction experiments was 4s. The
146 images were processed using Fit2d [50]. Each image was integrated in 5° azimuthal (ψ)
147 sectors, for a total of 72 patterns per image. The sets of patterns were further analyzed
148 with MAUD software package [55] to determine structural parameters.

149 In ideal conditions, the geometry of the diamond anvil cell imposes a cylindrical
150 symmetry of stress and strain at the center of the sample chamber (i.e. along the culets'
151 axial direction). The stress state far from the center of the culets is more complex [56].
152 For this reason at each pressure step the optimized position was determined by X-ray
153 absorption scans along the vertical and horizontal direction. An additional diffraction
154 image of gold was collected at each compression step for pressure calibration at high
155 temperatures [49].

156 In both the 673 K and 1073 K runs the sample was compressed at ambient temperature to
157 2.5 ± 1 GPa and then progressively heated to the target temperature at an average rate of
158 3.2 $^\circ\text{C}/\text{min}$ and 4.6 $^\circ\text{C}/\text{min}$, respectively. A total of 47 X-ray diffraction images were

This is the author's peer reviewed, accepted manuscript. However, the online version of record will be different from this version once it has been copyedited and typeset.
PLEASE CITE THIS ARTICLE AS DOI: 10.1063/1.5115350

159 collected along two isotherms at 673 K and 1073 K. The parameters of all the
160 experimental runs are reported in Table I.

161

162 D. Data analysis of radial diffraction data with MAUD

163 All radial X-ray diffraction images were analyzed using MAUD software package.

164 MAUD determines both crystal structure parameters, and texture by combining Rietveld
165 full-spectrum fitting and a selection of models to describe crystallite sizes, microstrains,
166 macroscopic stress and the crystals' preferred orientation [53, 57].

167 In radial X-ray diffraction experiments the sample is subject to strongly non-hydrostatic
168 macroscopic stress because it is loaded without any soft pressure transmitting medium.

169 The X-ray diffraction images display anisotropic strains caused by the uniaxial stress
170 applied to the sample. This results in non-circular Debye diffraction rings, with their
171 ellipticity being related to the amount of deviatoric stress and the elastic moduli of the

172 sample material. Specialized theories to describe non-hydrostatic crystal strains have
173 been developed to analyze the X-ray diffraction images collected from samples

174 compressed in the diamond anvil cell and other high-pressure devices [57-59]. In our

175 analysis here we are interested in the study of the (volume) compression of TaC, and we
176 correct for the effect of nonhydrostaticity by using the theory developed by Singh [58].

177 Here we assume that the TaC_{0.99} polycrystalline aggregate sample behaves as an

178 elastically isotropic material. Following the formulation presented by Singh [58] for the
179 isotropic aggregate case:

180
$$d_a(hkl) = d_p(hkl)[1 + (1 - 3\cos^2\psi)Q], \quad (1)$$

181 where $d_a(hkl)$ is the d-spacing of the (hkl) lattice planes family as determined in the
182 spectrum integrated at an angle ψ measured anticlockwise from the compression
183 direction. $d_p(hkl)$ is the d-spacing under hydrostatic stress (corresponding to pressure p),
184 and Q is a measure of the strain due to the deviatoric component of the stress. For
185 isotropic aggregates of elastically anisotropic materials, and assuming that stress is
186 homogeneous in the aggregate Singh [58] derives:

$$187 \quad \langle Q \rangle = t(1 + \nu)/3E = t/6G, \quad (2)$$

188 Where $\langle Q \rangle$ is the isotropic aggregate Q , averaged on all the diffracting lattice families
189 (see equation (1)), $t = \sigma_3 - \sigma_1$ is the difference between the normal stress along the
190 compression axis and perpendicular to it, ν is the average Poisson's ratio, E is the
191 Young's modulus of the isotropic aggregate sample, and G is the isotropic aggregate shear
192 modulus. The model of Singh [58] is incomplete for aggregates subject to plastic
193 deformation and with large density of defects [60]. However, equation (1) has been
194 shown to be useful to describe such experimental data, extract average stress levels [61],
195 and model plastic behavior of materials using more advanced methods [62].

196 The unit cell parameter a corresponding to the hydrostatic stress component is
197 determined from the spectrum at $\psi = 54.7$ degrees. The implementation of the model
198 available in MAUD allowed us to fix the values of ν and E and refine the values of σ_3
199 and σ_1 to fit the observed d-spacings. We calculated the value of $\langle Q \rangle$ by using equation
200 (2). This can finally be easily converted (see equation (1)) into the non-hydrostatic stress
201 contribution to the uncertainty on the unit cell parameter. The uncertainties due non-
202 hydrostatic conditions are in average of the order of 10^{-2} Å, substantially larger than the

203 estimated uncertainties on the values of the unit cell parameter refined with the full
204 spectrum fit which are of the order of 10^{-4} Å.

205 A typical X-ray diffraction image collected in radial scattering geometry is shown in
206 Figure 2(a). The unrolled sequence of spectra integrated at 5 degree azimuthal-angle
207 steps (see methods) is presented in Figure 2(b) together with the fit result.

208 In both the experiments performed at 673 K and 1073 K pressure was determined by
209 fitting the unit cell parameter of gold, loaded together with the sample in the sample
210 chamber. The analysis of X-ray diffraction of gold was performed similarly to that of the
211 sample material itself. The stress/lattice strain analysis generally gave results of
212 deviatoric stress comparable with those of the TaC_{0.99} sample. In some few cases the fit
213 of stress and lattice strain of gold did not converge to consistent results due to lower than
214 average gold diffraction signal.

215 The 3 X-ray diffraction images collected at 6.0, 6.8 and 8.2 GPa at 673 K and the 5 ones
216 collected at 1073 K from 32.9 to 38.8 GPa show a deviation from the ideal geometry,
217 with a maximum of lattice strains in a direction tilted with respect to the diamond anvil
218 axis (Figure 3). Non-ideal stress conditions are typically due to gasket partial failure at
219 the highest pressures (as in the case of the 1073 K isotherm) or, less frequently, at the
220 lowest pressures, at the first contact between the diamond culets and the ceramic gasket
221 (as in the case of the 673 K isotherm). Nevertheless, we performed a full analysis also of
222 these images and we will discuss the results below.

223 All parameters determined by Rietveld analysis of the diffraction images of TaC_{0.99} in the
224 two radial X-ray diffraction experimental runs are reported in Table II.

225

This is the author's peer reviewed, accepted manuscript. However, the online version of record will be different from this version once it has been copyedited and typeset.
PLEASE CITE THIS ARTICLE AS DOI: 10.1063/1.5115350

226 E. P-V-T equation of state analysis
227 A third order Birch-Murnaghan P-V equation of state [63] was fitted to the unit cell
228 volumes of TaC_{0.99} measured in the experiments performed in axial geometry and quasi-
229 hydrostatic stress. Pressures were determined from the unit cell volume of gold loaded in
230 the diamond anvil cell together with the sample [49]. The pressure - volume data were
231 weighted by the pressure uncertainties on the measurements of both gold and TaC_{0.99}
232 propagated from the uncertainties of their respective experimentally determined unit cell
233 volumes.
234 The three coefficients of the third order Birch-Murnaghan equation are the unit cell
235 volume at ambient conditions V_0 , the isothermal bulk modulus at ambient conditions K_{T0}
236 and its isothermal pressure derivative at ambient conditions $(\partial K_T/\partial P)_{T0}$. We fixed the
237 value of V_0 to the one we measured at the GFZ (see above) and we refined the values of
238 K_{T0} and $(\partial K_T/\partial P)_{T0}$. The individual data points used in the fit are reported in Table III
239 (“TaC-Ne”). In the fit we did not consider all the data points collected in decompression,
240 however we will mention, in the discussion, their effect on the fit results. After the first
241 decompression step the piston and cylinder of the diamond anvil cell were jammed. We
242 observed a sudden decrease of sample (and Au standard) unit cell volume between each
243 of the decompression points. The decompression volume – pressure data do not plot on
244 the compression dataset, even though they overlap within reciprocal pressure
245 uncertainties. Our interpretation is that, due to the sudden stress release, the stress field
246 applied to the sample was different with respect to that generated by the smooth stress
247 increase in compression, and the anomalous stress condition affected the pressure
248 determination. The last data point, collected at 1 bar after complete pressure release,

This is the author's peer reviewed, accepted manuscript. However, the online version of record will be different from this version once it has been copyedited and typeset.
PLEASE CITE THIS ARTICLE AS DOI: 10.1063/1.5115350

249 overlaps with the ambient conditions X-ray diffraction measurement and refinements
250 performed at the GFZ (see Figure 4).
251 The pressure volume data of TaC_{0.99} collected in radial diffraction geometry along the
252 two high temperature isotherms at 673 K and 1073 K were used to fit the parameters of
253 the Birch-Murnaghan-Debye P-V-T equation of state (e.g. [64]). Pressures were
254 determined from the measured unit cell volume of gold loaded in the diamond anvil cell
255 together with the sample. Error propagation of the uncertainties on sample and gold
256 experimental unit cell volumes was performed using the same strategy as for the room
257 temperature quasi-hydrostatic experimental dataset. We additionally weighted the data of
258 the high temperature runs (performed without soft pressure transmitting medium) by
259 propagating the additional volume strain caused to the uniaxial stress present in the
260 sample chamber (see section about Q – lattice strains analysis). The uncertainty on
261 temperature in the experimental setup used in this study is estimated to be ± 20 K at 673
262 K and ± 60 K at 1073 K [53].
263 The coefficients of the Birch-Murnaghan-Debye equation are V_0 , K_{T0} and $(\partial K_T/\partial P)_{T0}$
264 for the reference isotherm, which we fixed to be the ambient temperature isotherm. Three
265 thermal parameters were refined: the Grüneisen parameter at ambient conditions γ_0 , its
266 logarithmic volume derivative $q = (\partial \ln \gamma / \partial \ln V)_T$, and the Debye temperature at
267 ambient conditions θ_0 . Due to our limited dataset we fixed the initial unit cell volume of
268 the reference isotherm (V_0) to our own measurement result and the value of θ_0 to $567 \pm$
269 10 K which is the average of the available literature data [19, 24, 30, 31, 36, 39]
270 excluding the two extreme values [34, 37]. We thus refined the value of q and γ_0 , for
271 which the extant published results are in strong disagreement [17, 31, 36].

272 The whole dataset used to fit the parameters of the equation of state of TaC_{0.99} are
273 reported in Table II.

274

275 **III. RESULTS**

276 A. Isothermal equation of state of TaC_{0.99} at 296 K

277 The unit-cell volumes determined in the quasi-hydrostatic experiment are reported in
278 Table II. The compression curve is plotted in Figure 4. The third order Birch-Murnaghan
279 fit of our data yields $K_{0T} = 305 \pm 5$ GPa and $(\partial K_T / \partial P)_{T_0} = 6.1 \pm 0.5$, where K_{0T} is the
280 initial bulk modulus and $(\partial K_T / \partial P)_{T_0}$ is its initial pressure derivative. We performed our
281 fit by fixing V_0 (the initial unit-cell volume) to the value of 88.478 \AA^3 based on our
282 measurement at ambient pressure. The root mean square (RMS) misfit of the pressure
283 dataset is 0.29 GPa. We tested the effect of including the three decompression data (these
284 collected at 38.9, 32.0 and 18.8 GPa) in the fitted dataset. The fitted coefficients are
285 insensitive, within estimated uncertainties, to the inclusion of the decompression data.
286 However, the RMS misfit increases by more than 20% by adding these three data points,
287 and we decided to exclude them in our final fit (see Table II). The model isothermal
288 compression curve is plotted as a solid line in Figure 4.

289

290 B. P-V-T equation of state of TaC_{0.99}

291 The high-temperature unit-cell volumes dataset (Table II) combined with the parameters
292 of the ambient temperature isotherm were used to fit the thermal coefficients of a Birch-
293 Murnaghan-Debye equation of state. We did not include in the dataset the data collected
294 at 6.0, 6.8 and 8.2 GPa and 673 K and the 5 ones collected at 1073 K from 32.9 to 38.8

295 GPa (see also discussion). In the fit we fixed the value of θ_0 to the value of 570 ± 10 K
296 averaged between the available literature data (see methods above). The fit yields an
297 initial value of the Grüneisen parameter $\gamma_0 = 1.2 \pm 0.1$. The value of the logarithmic
298 pressure derivative of the Grüneisen parameter (q) is poorly constrained by the current
299 dataset and the best fit value is $q = 1 \pm 2$. The RMS pressure misfit of the full high
300 temperature dataset is equal to 0.46 GPa. The complete set of coefficient of the pressure-
301 volume-temperature equation of state of TaC_{0.99} based on our experimental results is
302 reported in Table III. The experimental unit-cell volumes and the model isotherms at 296
303 K, 673 K and 1073 K are plotted in Figure 5.

304

305 **IV. DISCUSSION**

306 A. Isothermal equation of state of TaC_{0.99} at 296 K

307 The values of $K_{0T} = 305 \pm 5$ and $(\partial K_T / \partial P)_{T_0} = 6.1 \pm 0.5$ constrained by our new quasi-
308 hydrostatic dataset compare well with the available computational and experimental
309 results for TaC_x (Table IV).

310 Several ab initio DFT computational studies have investigated the elastic properties of
311 TaC [6, 13, 15, 18, 33-39]. The values of the ambient pressure bulk modulus are
312 generally similar in all the studies when the same approximation is used for the
313 exchange-correlation electronic interaction. The average for the studies using the
314 generalized gradient approximation (GGA) is 315 ± 16 GPa and overlaps with our result
315 within reciprocal 1σ uncertainties. One of the computational studies [33] combines DFT
316 calculations and experimental ultrasonic interferometry data, for only two of the three
317 elastic stiffness coefficients of TaC. Using the elastic anisotropy expressed as the Zener

This is the author's peer reviewed, accepted manuscript. However, the online version of record will be different from this version once it has been copyedited and typeset.
PLEASE CITE THIS ARTICLE AS DOI: 10.1063/1.5115350

318 anisotropy ratio $A = 2C_{44}/(C_{11} - C_{12})$ [65], from their calculations we can estimate the
319 value of the experimental bulk modulus $K_{0S} = 310$ GPa, which agrees with our result
320 within 1σ . Here we point out that the difference between the isothermal bulk modulus
321 K_{0T} and the isentropic bulk modulus K_{0S} expressed by the thermodynamic relationship
322 $K_{0S} = K_{0T}(1 + \alpha\gamma T)$ (where α is the thermal expansion coefficient, and γ is the
323 Grüneisen parameter) in the case of TaC is of the order of 3 ± 1 GPa, which is
324 comparable with the uncertainties of all the existing experimental studies (Table IV).
325 Our best fit K_{0T} is at the lower end of the values of isothermal and isentropic bulk
326 modulus reported in the literature except for a single-crystal ultrasonics study of TaC_{0.90}
327 [29] and a neutron inelastic scattering study of single-crystal TaC [17] which yield $K_{0S} =$
328 217 ± 12 GPa and $K_{0S} = 283$ GPa, respectively. The three studies performed on TaC_{0.99},
329 present values of the isentropic bulk modulus K_{0S} between 345 GPa, and 317 GPa [28,
330 30, 66] all calculated by extrapolation to full density of ultrasonic experimental studies of
331 porous ceramic materials. If we consider all the available data from elasticity studies
332 including a study of TaC_{0.98} [31] the average value of 335 ± 13 GPa is compatible with
333 our fitted value only at 3σ uncertainty level.
334 Only three experimental and three computational studies investigated the pressure
335 dependence of the elastic moduli of TaC_x [16, 31-33, 36, 37]. The pressure derivatives
336 $(\partial K_T/\partial P)_{T_0}$ based on experimental studies [31, 32, 37] are equal to 4.97 ± 0.27 , $4.0 \pm$
337 0.4 and 4 respectively, and are substantially different from our result. However, the
338 pressure derivative presented in [31] is calculated from ultrasonics pulse-echo
339 measurements of a compressed porous sample without direct measurements of the sample
340 volume. The value reported by [37] is based on a high-pressure X-ray diffraction study of

This is the author's peer reviewed, accepted manuscript. However, the online version of record will be different from this version once it has been copyedited and typeset.
PLEASE CITE THIS ARTICLE AS DOI: 10.1063/1.5115350

341 nano-particle TaC, which could have a different elastic behavior with respect to the bulk
342 material (see for instance the case of MgO [67]), and it has been fixed in the data
343 analysis. The results of [32] are based on a similar approach as the one used in the present
344 study and the large disagreement deserves a more detailed explanation. Liermann and
345 coauthors [32] performed high-pressure X-ray powder diffraction of TaC_{0.98} compressed
346 in the diamond anvil cell using Al as a pressure transmitting medium. Even though Al is
347 a metal with low shear modulus at ambient conditions, it represents a strong pressure
348 medium if compared to Ne at pressures of tens of GPa. The use of strong pressure media
349 unavoidably produces deviatoric stress in the sample chamber. In axial X-ray diffraction
350 geometry the crystallites which contribute to the measured signal are those with
351 diffracting vectors (the directions normal to the diffracting lattice planes) close to
352 perpendicular to the diamond axes, and thus subject to deviatoric extension (relative to
353 the ideal hydrostatic strain) [58]. This causes underestimation of volume compression and
354 overestimation of the material bulk modulus [67, 68]. In addition to this, the value of bulk
355 modulus and pressure derivative at ambient conditions obtained by fitting high-pressure
356 X-ray diffraction results suffer from trade-offs between the two coefficients of the fitted
357 equation of state [69]. In order to better compare the results of the two studies we have
358 plotted the difference between the P-V isotherms calculated using the two sets of
359 parameters and a common starting volume (Figure 6). This procedure corresponds to
360 comparing pressures along the two isotherms at the same values of compression. The
361 difference between the two compression curves is within three times the average
362 uncertainty of our data if we include the error propagated from the unit-cell volume
363 uncertainty. If we consider that the experimental uncertainties on pressure and unit-cell

This is the author's peer reviewed, accepted manuscript. However, the online version of record will be different from this version once it has been copyedited and typeset.
PLEASE CITE THIS ARTICLE AS DOI: 10.1063/1.5115350

364 volume in [32] are of the same order of magnitude as the one in our dataset, the
365 disagreement between the two isothermal equations of state is within 2σ reciprocal
366 uncertainties. The similarity between the compression curves of $\text{TaC}_{0.99}$ and $\text{TaC}_{0.98}$
367 suggests that, within experimental uncertainties, the isothermal compressibility of TaC_x at
368 300 K is only marginally sensitive to low levels of nonstoichiometry ($0.98 \leq x < 1$).
369 The pressure derivative of the bulk modulus from the four ab initio computational studies
370 with local density approximation (LDA) [33], generalized gradient approximation (GGA)
371 [36] and with both approximations [16, 37] is in all cases substantially smaller (between
372 29% and 42%) than our result. However, this is partially compensated by their larger bulk
373 modulus at room pressure. The discrepancy between our experimental results and ab
374 initio computations could be due to the presence, in our sample material, of a complex
375 defect structure in addition to slight non-stoichiometry, which includes dislocations, grain
376 boundaries and microstrains associated to them. Indeed it has been observed that carbon-
377 defective TaC_x ceramics show higher mechanical strength than stoichiometric TaC [3].
378 The characterization of defects states and their energetics in TaC has been subject of
379 several computational and theoretical studies [70, 71]. A recent study has shown that
380 increasing C vacancies concentration reduces the elastic moduli of TaC_x [72]. However,
381 it is not yet clear what effect this deficiency has on the pressure dependence of bulk
382 modulus. The isothermal compression curves of all the existing high-pressure studies of
383 TaC_x [16, 31-33, 36, 37] are calculated with the same procedure as for [32] (see above)
384 and compared with ours in Figure 6.
385
386 B. P-V-T equation of state of $\text{TaC}_{0.99}$

This is the author's peer reviewed, accepted manuscript. However, the online version of record will be different from this version once it has been copyedited and typeset.
PLEASE CITE THIS ARTICLE AS DOI: 10.1063/1.5115350

387 Our full high-pressure / high-temperature dataset places a strong constrain on the value of
388 $\gamma_0 = 1.2 \pm 0.1$. In the framework of the Birch-Murnaghan-Debye model this coefficient is
389 the thermodynamic Grüneisen parameter at ambient conditions. This value is obtained by
390 fitting both our full dataset, or after removing the 3 data points at 6.0, 6.8 and 8.2 GPa
391 and 673 K and the 5 data for 32.9, 34.9 36.1, 37.9 and 38.8 GPa and 1073 K due to their
392 non-ideal geometry (see section 2. Materials and Methods). Our best-fit value of
393 γ_0 compares very well with the value of the elastic Grüneisen parameter $\gamma_{el} = 1.22$
394 determined for polycrystalline TaC_{0.98} by ultrasonic techniques [31]. However, the elastic
395 Grüneisen parameter is the average value of the volume dependence of the acoustic
396 phonon frequencies at the Brillouin zone center, a parameter which is different from the
397 thermodynamic Grüneisen parameter $\gamma_{th} = \alpha K_S / (\rho C_p)$ (where α is the volume thermal
398 expansion coefficient, K_S is the isentropic bulk modulus, ρ is density and C_p is the
399 specific heat at constant pressure) which controls the thermal pressure contribution in the
400 P-V-T equation of state. The value of the thermodynamic Grüneisen parameter at
401 ambient conditions calculated from the published thermoelastic properties of TaC_x (Table
402 V) ranges between 1.47 and 2.34, that is 30% to 90% larger than the best-fit value to our
403 experimental dataset. The reason of this difference is clearly due to the limitations of the
404 Birch-Murnaghan-Debye model to describe the thermal energy contribution in TaC_{0.99}.
405 The high temperature study of the elastic properties of TaC_{0.99} by Jun and Shaffer [30]
406 shows that the thermodynamic Grüneisen parameter has very strong temperature
407 dependence below 600 K at ambient pressure with a decrease from 1.48 at 300 K to 1.2 at
408 600 K, and then it remains almost constant at the value of 1.2 at temperatures as high as
409 1500 K. On the opposite, Peng et al. [36] who use the Debye model and a quasi-harmonic

This is the author's peer reviewed, accepted manuscript. However, the online version of record will be different from this version once it has been copyedited and typeset.
PLEASE CITE THIS ARTICLE AS DOI: 10.1063/1.5115350

410 approximation obtain γ slowly increasing with temperature at ambient pressure (Figure
411 7).

412 The quasi-harmonic approximation underlying our equation of state assumes that γ is not
413 explicitly temperature dependent (it is indeed temperature dependent through its volume
414 dependence). This approximation seems to hold for TaC_{0.99} at temperatures above 600 K.

415 The result of the fit to our 673 K and 1073 K isotherms constrains an effective high-
416 temperature value of the ambient pressure thermal Grüneisen parameter, which is more
417 consistent with the results of high temperature ultrasonics measurements [30] rather than
418 room temperature ultrasonics [30, 31] or computations [36].

419 The value of q , the logarithmic volume derivative of the Grüneisen parameter, is poorly
420 constrained by our high-temperature dataset. The best-fit value of q is strongly affected
421 by the highest pressures data along the 1073 K isotherm. The fit to our full dataset yields
422 $q = -0.3 \pm 1.4$, while excluding the non-ideal data points at 32.9, 34.9, 36.1, 37.9 and 38.8
423 GPa at 1073 K from the fit yields $q = 1 \pm 2$ (see also results). The average RMS misfit of
424 the full dataset (50 data points) is 0.46 GPa, that of the non-ideal 5 data points is 0.59
425 GPa while that of all the others is 0.44 GPa. The non-ideal data points have a 34% higher
426 disagreement with the fit than all the rest of the dataset. We interpret this as a systematic
427 bias probably connected to the non-ideal geometry in these measurements, and we
428 consider the result of the analysis of the reduced dataset as our best fit result. The fit
429 results are instead unaffected by including or excluding the 3 non-ideal data points at 6.0,
430 6.8 and 8.2 GPa along the 673 K isotherm. Based on the overall fit of the model
431 isotherms at 673 K and 1073 K, a value of q close to unity is a good approximation of the

432 logarithmic volume sensitivity of γ in the high temperature regime ($T > 600$ K). This
433 corresponds to:

$$434 \quad \gamma(V) \cong \gamma_0^{HT} (V/V_0), \quad (4)$$

435 where γ_0^{HT} is the high-temperature, ambient pressure value of $\gamma = 1.2 \pm 0.1$ based on our
436 fit (see discussion above), V represents volume and V_0 the volume at ambient conditions.

437 In conclusion, our P-V-T model is able to successfully describe the pressure – volume –
438 temperature relationship for TaC_{0.99} at 296 K and in the high-temperature range between
439 673 and 1073 K at pressures as high as 35 GPa, while we expect that it fails to describe
440 the high-pressure behavior of TaC_{0.99} in the ~300-600 K temperature regime, especially
441 at low pressures. The parameters for the high-temperature equation of state of TaC_{0.99} are
442 reported in Table III. The extant published results for TaC_x are reported for comparison
443 in Tables IV and V.

444

445 **V. CONCLUSIONS**

446 Our extensive experimental investigation gives new information about the compression
447 behavior of TaC_{0.99} under very high pressures and temperatures in the diamond anvil cell.

448 a) We have constrained the parameters of the P-V-T equation of state of TaC_{0.99} to 1073
449 K and 32 GPa. The ambient pressure derivative of the bulk modulus is substantially
450 higher (50%) with respect to previous studies at the same composition. The
451 thermodynamic Grüneisen parameter refined from our results is lower than the available
452 data at ambient conditions, and it seems to be consistent with the experimental high
453 temperature limit. The approach used here of determining isothermal EOS data from x-
454 ray diffraction data collected in the radial diffraction geometry under nonhydrostatic

455 conditions is novel and shows the potential of this technique, in particular the use of
456 ceramic gaskets that are more stable at higher temperatures and the lack of a hydrostatic
457 compression medium. Thus, the technique is ideally suited to characterize the thermal-
458 elastic properties of hard materials such as transition metal carbides.

459

460 ACKNOWLEDGMENTS

461 Part of this research was supported through the projects “GeoMaX” funded under the
462 Emmy-Noether Program of the German Science Foundation (MA4534/3-1) as well as
463 grant MA4534/4-1. HM acknowledges support from the Bavarian Academy of Sciences.
464 We acknowledge technical assistance by A. Ehnes and I. Schwark from the sample
465 environment group at PETRA III within the framework of the Extreme Conditions
466 Science Infrastructure ECSI). We thank J. Mainberger for preparing the carbides samples
467 for the carbon analysis and Martin Harms for proofreading and reformatting the reference
468 list.

469

470 References

- 471 [1] M. J. Gasch, D. T. Ellerby, and S. M. Johnson, in *Handbook of Ceramic Composites*
472 edited by N. P. Bansal (Kluwer Academic Publishers, Boston MA, 2005), pp. 197-
473 224.
- 474 [2] K. Upadhyaya, J. M. Yang, and W. P. Hoffmann, *Am. Ceram. Soc. Bull.*, **58**, 51 (1997).
- 475 [3] L. E. Toth, *Transition Metal Carbides and Nitrides* (Academic Press, New York and
476 London, 1971).
- 477 [4] W. S. Williams, *Mater. Sci. Eng.*, **A105/106**, 1 (1988).

This is the author's peer reviewed, accepted manuscript. However, the online version of record will be different from this version once it has been copyedited and typeset.
PLEASE CITE THIS ARTICLE AS DOI: 10.1063/1.5115350

- 478 [5] K. Hackett, S. Verhoef, R. A. Cutler, and D. K. Shetty, *J. Am. Ceram. Soc.*, **92**, 2404
479 (2009).
- 480 [6] X.-X. Yu, C. R. Weinberger, and G. B. Thompson, *Acta Mater.*, **80**, 341 (2014).
- 481 [7] B. D. Diwan, *Can. J. Phys.*, **92**, 415 (2014).
- 482 [8] A. L. Bowman, *J. Phys. Chem.*, **65**, 1596 (1961).
- 483 [9] A. I. Gusev, A. A. Rempel, and V. N. Lipatnikov, *J. Phys. Condens. Matter*, **8**, 8277,
484 1996.
- 485 [10] K. Nakamura and M. Yashima, *Mater. Sci. Eng. B*, **148**, 69 (2008).
- 486 [11] J. R. Cooper and R. L. Hansler, *J. Chem. Phys.*, **39**, 248 (1963).
- 487 [12] G. Santoro and R. T. Dolloff, *J. Appl. Phys.*, **39**, 2293 (1968).
- 488 [13] E. I. Isaev, S. I. Simak, I. A. Abrikosov, R. Ahuja, Y. K. Vekilov, M. I. Katsnelson,
489 A. I. Lichtenstein, and B. Johansson, *J. Appl. Phys.*, **101**, 123519 (2017).
- 490 [14] B. M. Klein, L. L. Boyer, and D. A. Papaconstantopoulos, *Solid State Commun.*, **20**,
491 937 (1976).
- 492 [15] H. Li, L. Zhang, Q. Zeng, K. Guan, K. Li, H. Ren, S. Liu, and L. Cheng, *Solid State*
493 *Commun.*, **151**, 602 (2011).
- 494 [16] M. Sahnoun, C. Daul, M. Driz, J. C. Parlebas, and C. Demangeat, *Comput. Mater.*
495 *Sci.*, **33**, 175 (2005).
- 496 [17] H. G. Smith and W. Gläser, *Phys. Rev. Lett.*, **25**, 1611 (1970).
- 497 [18] W. Weber, *Phys. Rev. B* **8**, 5082 (1973).
- 498
499 [19] C. P. Kempter, *Phys. Status Solidi B*, **36**, K137 (1969).
- 500 [20] C. R. Houska, *J. Am. Ceram. Soc.*, **47**, 310 (1964).
- 501 [21] K. K. Kelley, *J. Am. Chem. Soc.*, **62**, 818 (1940).

This is the author's peer reviewed, accepted manuscript. However, the online version of record will be different from this version once it has been copyedited and typeset.
PLEASE CITE THIS ARTICLE AS DOI: 10.1063/1.5115350

- 502 [22] R. O. Elliott and C.P. Kempter, *J. Phys. Chem.*, **62**, 630 (1958).
- 503 [23] C. K. Jun and P.T.B. Shaffer, *J. Less Common Met.*, **24**, 323 (1971).
- 504 [24] K. Frisk and A. Fernández Guillermet, *J. Alloy. Compd.*, **238**, 167 (1996).
- 505 [25] A. Krajewski, L. D'Alessio, and G. De Maria, *Cryst. Res. Technol.*, **33**, 341(1998).
- 506 [26] C. Kral, W. Lengauer, D. Rafaja, and P. Ettmayer, *J. Alloy. Compd.*, **265**, 215
- 507 (1998).
- 508 [27] A. Friedrich, B. Winkler, E. A. Juarez-Arellano, and L. Bayarjargal, *Mater.*, **4**, 1648
- 509 (2011).
- 510 [28] H. L. Brown, P. E. Armstrong, and C. P. Kempter, *J. Chem. Phys.*, **45**, 547 (1996).
- 511 [29] R. W. Bartlett and C. W. Smith, *J. Appl. Phys.*, **38**, 5428 (1967).
- 512 [30] C. K. Jun and P. T. B. Shaffer, *J. Less Common Met.*, **23**, 367 (1971).
- 513 [31] S. P. Dodd, M. Cankurtaran, and B. James, *J. Mater. Sci.*, **38**, 1107 (2003).
- 514 [32] H. P. Liermann, A. K. Singh, B. Manoun, S. K. Saxena, and C. S. Zha, *Int. J.*
- 515 *Refract. Met. Hard Mater.*, **23**, 109 (2005).
- 516 [33] L. López-de-la-Torre, B. Winkler, J. Schreuer, K. Knorr, and M. Avalos-Borja, *Solid*
- 517 *State Commun.*, **134**, 245 (2005).
- 518 [34] Z. Wu, X.-J. Chen, V. V. Struzhkin, and R. E. Cohen, *Phys. Rev. B*, **71**, 214103
- 519 (2005).
- 520 [35] X.-G. Lu, M. Selleby, and B. Sundman, *Acta Mater.*, **55**, 1215 (2007).
- 521 [36] F. Peng, L. Han, H. Fu, and X. Cheng, *Phys. Status Solidi B*, **246**, 1590 (2009).
- 522 [37] H.-H. Chen, Y. Bi, H.-K. Mao, J.-A. Xu, L. Liu, Q.-M. Jing, Z. Li, X.-R. Chen, Q.-
- 523 and M. Wang, *Int. J. Refract. Met. Hard Mater.*, **41**, 627 (2013).
- 524 [38] Y. Liu, Y. Jiang, R. Zhou, and J. Feng, *J. Alloy. Compd.*, **582**, 500 (2014).

This is the author's peer reviewed, accepted manuscript. However, the online version of record will be different from this version once it has been copyedited and typeset.
PLEASE CITE THIS ARTICLE AS DOI: 10.1063/1.5115350

- 525 [39] G. Sai Gautam and K. C. Hari Kumar, *J. Alloy. Compd.*, **587**, 380 (2014).
- 526 [40] H.-R. Wenk, S. Matthies, R. J. Hemley, H.-K. Mao, and J. Shu, *Nature*, **405**, 1044
527 (2000).
- 528 [41] S. Merkel, A. K. McNamara, A. Kubo, S. Speziale, L. Miyagi, Y. Meng, T. S.
529 Duffy, and H.-R. Wenk, *Science*, **316**, 1729 (2007).
- 530 [42] H. Marquardt and L. Miyagi, *Nat. Geosci.*, **8**, 311 (2015).
- 531 [43] T. S. Duffy, G. Shen, D. L. Heinz, J. Shu, Y. Ma, H.-K. Mao, R. J. Hemley, and A.
532 K. Singh, *Phys. Rev. B*, **60**, 15063 (1999).
- 533 [44] B. Kiefer, S. R. Shieh, T. S. Duffy, and T. Sekine, *Phys. Rev. B*, **72**, 014102 (2005).
- 534 [45] H. Dong, D. He, T. S. Duffy, and Y. Zhao, *Phys. Rev. B*, **79**, 014105 (2009).
- 535 [46] S. Merkel, H.-P. Liermann, L. Miyagi, and H.-R. Wenk, *Acta Mater.*, **61**, 5144
536 (2013).
- 537 [47] H.-K. Mao, R. J. Hemley, and A. L. Mao, in *Advances in high pressure research in*
538 *condensed matter: proceedings of the international conference on condensed matter*
539 *under high pressures* edited by B. K. Godwal, (NISCOM, New Delhi, India, 1997),
540 pp. 12-19.
- 541 [48] H.-K. Mao, J. Xu, and P. M. Bell, *J. Geophys. Res.*, **91**, 4673, 1986.
- 542 [49] Y. Fei, A. Ricolleau, M. Frank, K. Mibe, G. Shen, and V. Prakapenka, *Proc. Natl.*
543 *Acad. Sci.*, **104**, 9182 (2007).
- 544 [50] A. P. Hammersley, S. O. Svensson, M. Hanfland, A. N. Fitch, and D. Hausermann,
545 *High Press. Res.*, **14**, 235 (1996).
- 546 [51] A. Le Bail, H. Duroy, and J. L. Fourquet, *Mater. Res. Bull.*, **23**, 447 (1988).

This is the author's peer reviewed, accepted manuscript. However, the online version of record will be different from this version once it has been copyedited and typeset.
PLEASE CITE THIS ARTICLE AS DOI: 10.1063/1.5115350

- 547 [52] L. Lutterotti, S. Matthies, H.-R. Wenk, A. S. Schultz, and J. W. Richardson, *J. Appl.*
548 *Phys.*, **81**, 594 (1997).
- 549 [53] H.-P. Liermann, S. Merkel, L. Miyagi, H.-R. Wenk, G. Shen, H. Cynn, and W.J.
550 Evans, *Rev. Sci. Instrum.*, **80**, 104501 (2009).
- 551 [54] H.-P. Liermann, Z. Konôpková, W. Morgenroth, K. Glazyrin, J. Bednarčík, E. E.
552 McBride, S. Petitgirard, J. T. Delitz, M. Wendt, Y. Bican, A. Ehnes, I. Schwark, A.
553 Rothkirch, M. Tischer, J. Heuer, H. Schulte-Schrepping, T. Kracht, and H. Franz, *J.*
554 *Synchrotron Radiat.*, **22**, 908 (2015).
- 555 [55] H.-R. Wenk, L. Lutterotti, P. Kaercher, W. Kaniitpanyacharoen, L. Miyagi, and R.
556 Vasin, *Powder Diffr.*, **29**, 220 (2014).
- 557 [56] C.-M. Sung, C. Goetze, and H.-K. Mao, *Rev. Sci. Instrum.*, **48**, 1386 (1977).
- 558 [57] A. K. Singh and G. C. Kennedy, *J. Appl. Phys.*, **45**, 4686 (1974).
- 559 [58] A. K. Singh, *J. Appl. Phys.*, **73**, 4278 (1993).
- 560 [59] T. Uchida, N. Funamori, and T. Yagi, *J. Appl. Phys.*, **80**, 739 (1996).
- 561 [60] S. Merkel, N. Miyajima, D. Antonangeli, G. Fiquet, and T. Yagi, *J. Appl. Phys.*, **100**,
562 023510 (2006).
- 563 [61] H. Dong, D. He, T.S. Duffy, and Y. Zhao, *Phys. Rev. B*, **79**, 014105 (2009).
- 564 [62] S. Merkel, C.N. Tomé, and H.R. Wenk, *Phys. Rev. B*, **79**, 064110 (2009).
- 565 [63] F. Birch, *Phys. Rev.*, **71**, 809 (1947).
- 566 [64] T. S. Duffy and Y. Wang, in *Ultrahigh-Pressure Mineralogy: Physics and*
567 *Chemistry of the Earth's Deep Interior* edited by R.J. Hemley, *Reviews in*
568 *Mineralogy* Vol. 37 (Mineralogical Society of America, Washington DC, 1998), pp.
569 425-457.

This is the author's peer reviewed, accepted manuscript. However, the online version of record will be different from this version once it has been copyedited and typeset.
PLEASE CITE THIS ARTICLE AS DOI: 10.1063/1.5115350

- 570 [65] C. Zener, *Elasticity and Anelasticity in Metals* (University of Chicago Press,
571 Chicago, 1948).
- 572 [66] V. G. Bukatov, V. I. Knyazev, O. S. Korostin, and V. M. Baranov, *Inorg. Mater.*, **11**,
573 310 (1975).
- 574 [67] H. Marquardt, S. Speziale, K. Marquardt, H. J. Reichmann, Z. Konôpková, W.
575 Morgenroth, and H.-P. Liermann, *J. Appl. Phys.*, **110**, 113512 (2011).
- 576 [68] A. K. Singh, *High Temp. High Press.*, **10**, 41 (1978).
- 577 [69] J. D. Bass, R. C. Liebermann, D. J. Weidner, and S. J. Finch, *Phys. Earth Planet.*
578 *Inter.*, **25**, 140 (1981).
- 579 [70] G. R. Gruzalski, and D. M. Zehner, *Phys. Rev. B*, **34**, 3841 (1986).
- 580 [71] J.-H. Jhi, S. G. Louie, M. L. Cohen, and J. Ihm, *Phys. Rev. Lett.*, **86**, 3348 (2001).
- 581 [72] X.-X. Yu, G. B. Thompson, and C. R. Weinberger, *J. Europ. Ceram. Soc.*, **35**, 95
582 (2015).
- 583
- 584
- 585

586 Figure captions

587 Figure 1. X-ray diffraction of TaC_{0.99} compressed in Ne pressure transmitting medium to
588 19.7 GPa at ambient temperature. (a) X-ray diffraction image; (b) Integrated pattern
589 and LeBail calculated best fit spectrum. The bars underneath the pattern are the
590 calculated positions of the diffraction peaks of TaC and of gold (used as an internal
591 pressure standard). The misfit is also plotted as the difference between calculated and
592 observed amplitudes.

593 Figure 2. Radial X-ray diffraction of TaC_{0.99} compressed without pressure transmitting
594 medium to 29.4 GPa at 1073 K. (a) X-ray diffraction image; (b) Sequence of patterns
595 integrated from 5° azimuthal sectors and the fit model calculated by MAUD software
596 (the arrows indicate the compression direction parallel to the diamond anvils axes).

597 Figure 3. Example of radial X-ray diffraction measurement in non-ideal sample
598 geometry. (a) Sequence of azimuthally integrated patterns from the radial X-ray
599 diffraction image collected at 38.8 GPa and 1073 K. The direction of the diamond
600 axes (red arrow) does not correspond to that of maximum strain of the sample (white
601 arrow); (b) Ideal case (29.4 GPa and 1073 K) the direction of maximum strain
602 corresponds to the diamond axis direction.

603 Figure 4. Isothermal compression of TaC_{0.99} at ambient temperature (296 K). The dataset
604 used for the analysis is that of experiment “TaC-Ne” (see text). The data collected in
605 decompression were not used for the fit of the P-V equation of state.

606 Figure 5. P-V-T compression behavior of TaC_{0.99}. The data used for fitting are colored as
607 a function of the experimental temperature following the color scale displayed in the
608 legend. The curves are the best-fit model P-V isotherms at the temperatures of the 3

609 datasets (296 K, 673 K, 1073 K). The white-filled symbols correspond to data points
610 in non-ideal geometry (see text), which were not used for the fit.

611 Figure 6. Comparison of the 296 K P-V equation of state of $\text{TaC}_{0.99}$ with the other
612 available models for TaC_x compositions. The disagreement is expressed as the
613 difference between the pressures calculated for the different models and our equation
614 of state at the same values of Eulerian strain. The differences are plotted versus the
615 pressure calculated with our equation of state (in abscissa). In the legend “exp”
616 indicates experimental studies, “DFT” indicates computational studies using density
617 functional theory.

618 Figure 7. Temperature dependence $\text{TaC}_{0.99}$ thermodynamic Grüneisen parameter at
619 ambient temperature. The results from our P-V-T are compared with the other
620 available results from experimental and computational studies.

621

622 Tables titles

623 Table I. Experimental condition of the four X-ray diffraction datasets. “Cold compr.” is
624 the maximum sample pressure before starting heating.

625 Table II. Summary of the all the experimental results from all the three runs. “stdev P +
626 V-TaC” is the complete uncertainty on pressure including the propagation of the
627 uncertainty on the unit-cell volume of $\text{TaC}_{0.99}$. “ $\langle Q \rangle$ ” is the isotropic aggregate value
628 of Q , a measure of the strain due to the deviatoric component of the stress applied to
629 the sample (see main text). “PV fit” indicates whether the data points were used or
630 not in the isothermal (296 K) P-V equation of state fit. “PVT fit” indicates whether
631 the data points were used or not in the P-V-T equation of state fit.

This is the author's peer reviewed, accepted manuscript. However, the online version of record will be different from this version once it has been copyedited and typeset.
PLEASE CITE THIS ARTICLE AS DOI: 10.1063/1.5115350

632 Table III. Best fit parameters of the P-V-T equation of state of TaC_{0.99} based on our
633 experimental data.

634 Table IV. Comparison of our best-fit thermoelastic parameters for TaC_{0.99} and all the
635 available literature data. “E” is the isotropic aggregate Young’s modulus. “Poisson’s”
636 is the isotropic aggregate Poisson’s ratio. All the parameters refer to ambient
637 conditions. †The elastic coefficients are not presented in the original paper.

638 *Parameter fixed in the analysis of the data.

639 Table V. Summary of the available results about the thermal properties of TaC_x from the
640 literature.

641

This is the author's peer reviewed, accepted manuscript. However, the online version of record will be different from this version once it has been copyedited and typeset.
PLEASE CITE THIS ARTICLE AS DOI: 10.1063/1.5115350

642 Table I

Experiment	TaC-Ne	TaC-HT1	TaC-HT2
Diffraction geometry	Axial	Radial	Radial
X-ray Wavelength (Å)	0.2966	0.4847	0.4847
DAC type	Symmetric P-C	modif. Mao-Bell	modif. Mao-Bell
diamond anvil culet (μm)	300	300	300
P transmitting Medium	Ne	no	no
P calibrant	Au, ruby	Au	Au
Temperature (K)	296	673	1073
N data points	20	22	25
Max P (GPa)	43.6	33.6	38.8
Exp time (s)	20	4	4
Max membrane P (bar)	28.4	58.9	65.0
Exp duration (h)	3	5	6
Cold compr. (GPa)		2.4	2.6

643

This is the author's peer reviewed, accepted manuscript. However, the online version of record will be different from this version once it has been copyedited and typeset.
PLEASE CITE THIS ARTICLE AS DOI: 10.1063/1.5115350

644 Table II

Experiment	T (K)	P (GPa)	V (\AA^3)	stdev P + V TaC (GPa)	$\langle Q \rangle$	PV fit	PVT fit
TaC-Ne	296	5.1±0.1	87.06±0.01	0.19	--	yes	yes
TaC-Ne	296	6.4±0.2	86.71±0.02	0.31	--	yes	yes
TaC-Ne	296	10.3±0.1	85.79±0.02	0.22	--	yes	yes
TaC-Ne	296	11.6±0.1	85.47±0.02	0.20	--	yes	yes
TaC-Ne	296	14.5±0.3	84.81±0.02	0.35	--	yes	yes
TaC-Ne	296	17.3±0.5	84.21±0.04	0.67	--	yes	yes
TaC-Ne	296	19.7±0.6	83.82±0.04	0.82	--	yes	yes
TaC-Ne	296	22.2±0.6	83.35±0.04	0.84	--	yes	yes
TaC-Ne	296	24.6±0.5	82.91±0.04	0.74	--	yes	yes
TaC-Ne	296	27.1±0.4	82.43±0.04	0.66	--	yes	yes
TaC-Ne	296	29.5±0.5	82.02±0.04	0.76	--	yes	yes
TaC-Ne	296	31.6±0.5	81.64±0.01	0.60	--	yes	yes
TaC-Ne	296	34.1±0.6	81.21±0.01	0.64	--	yes	yes
TaC-Ne	296	36.4±0.8	80.83±0.01	0.82	--	yes	yes
TaC-Ne	296	38.4±0.6	80.48±0.01	0.66	--	yes	yes
TaC-Ne	296	40.8±0.8	80.07±0.01	0.81	--	yes	yes
TaC-Ne	296	43.6±0.7	79.63±0.01	0.77	--	yes	yes
TaC-Ne	296	38.9±0.8	80.47±0.01	0.83	--	no	yes
TaC-Ne	296	32.0±0.7	81.72±0.02	0.68	--	no	yes
TaC-Ne	296	18.8±1.0	84.11±0.04	1.06	--	no	yes
TaC-Ne	296	0.0001	88.478±0.003	0.001	--	yes	yes
TaC-HT1	673±10	7.4±0.3	86.95±0.10	0.68	0.0009	no	yes
TaC-HT1	674±10	6.0±0.3	87.10±0.11	0.70	0.0010	no	no
TaC-HT1	673±10	6.8±0.3	86.89±0.09	0.64	0.0011	no	no
TaC-HT1	673±10	8.2±0.3	86.68±0.09	0.66	0.0012	no	no
TaC-HT1	673±10	9.4±0.3	86.46±0.11	0.75	0.0014	no	yes
TaC-HT1	682±10	11.0±0.3	86.17±0.10	0.72	0.0015	no	yes
TaC-HT1	673±10	12.6±0.3	85.71±0.11	0.78	0.0018	no	yes
TaC-HT1	673±10	15.3±0.4	85.13±0.10	0.81	0.0022	no	yes
TaC-HT1	673±10	17.4±0.4	84.61±0.11	0.89	0.0024	no	yes

This is the author's peer reviewed, accepted manuscript. However, the online version of record will be different from this version once it has been copyedited and typeset.
PLEASE CITE THIS ARTICLE AS DOI: 10.1063/1.5115350

TaC-HT1	671±10	20.0±0.4	83.99±0.10	0.89	0.0030	no	yes
TaC-HT1	667±10	23.6±0.4	83.39±0.11	0.97	0.0035	no	yes
TaC-HT1	672±10	26.5±0.4	82.84±0.10	0.99	0.0040	no	yes
TaC-HT1	672±10	28.4±0.5	82.42±0.11	1.07	0.0041	no	yes
TaC-HT1	673±10	30.7±0.5	81.96±0.10	1.04	0.0044	no	yes
TaC-HT1	673±10	32.2±0.5	81.52±0.10	1.10	0.0046	no	yes
TaC-HT1	673±10	33.0±0.5	81.51±0.09	1.05	0.0047	no	yes
TaC-HT1	672±10	33.6±0.5	81.54±0.11	1.16	0.0042	no	yes
TaC-HT1	674±10	24.6±0.4	83.09±0.11	1.00	0.0014	no	yes
TaC-HT2	297	1.9±0.3	87.98±0.05	0.43	0.0006	no	yes
TaC-HT2	297	1.8±0.3	87.98±0.05	0.44	0.0005	no	yes
TaC-HT2	297	2.6±0.3	87.80±0.06	0.49	0.0007	no	yes
TaC-HT2	1073±10	2.9±0.2	88.57±0.13	0.67	0.0012	no	yes
TaC-HT2	1072±10	3.0±0.2	88.47±0.12	0.63	0.0017	no	yes
TaC-HT2	1074±10	3.0±0.2	88.46±0.12	0.64	0.0016	no	yes
TaC-HT2	1073±10	2.9±0.2	88.54±0.12	0.65	0.0013	no	yes
TaC-HT2	1069±10	2.9±0.2	88.54±0.13	0.65	0.0014	no	yes
TaC-HT2	1071±10	2.8±0.2	88.58±0.12	0.61	0.0015	no	yes
TaC-HT2	1072±10	2.9±0.2	88.66±0.12	0.64	0.0015	no	yes
TaC-HT2	1073±10	3.0±0.2	88.66±0.13	0.68	0.0016	no	yes
TaC-HT2	1073±10	3.1±0.2	88.68±0.13	0.66	0.0014	no	yes
TaC-HT2	1072±10	3.2±0.2	88.66±0.11	0.61	0.0015	no	yes
TaC-HT2	1056±10	3.2±0.2	88.59±0.12	0.63	0.0018	no	yes
TaC-HT2	1075±10	3.7±0.2	88.48±0.12	0.65	0.0020	no	yes
TaC-HT2	1074±10	11.3±0.3	86.29±0.11	0.75	0.0027	no	yes
TaC-HT2	1075±10	11.4±0.3	86.23±0.11	0.76	0.0029	no	yes
TaC-HT2	1073±10	12.0±0.3	86.08±0.13	0.85	0.0030	no	yes
TaC-HT2	1074±10	13.4±0.3	85.77±0.13	0.88	0.0033	no	yes
TaC-HT2	1073±10	14.7±0.3	85.49±0.12	0.85	0.0036	no	yes
TaC-HT2	1073±10	17.9±0.4	84.75±0.12	0.92	0.0039	no	yes
TaC-HT2	1072±10	20.7±0.4	84.20±0.13	0.99	0.0040	no	yes
TaC-HT2	1073±10	23.3±0.4	83.73±0.14	1.07	0.0041	no	yes
TaC-HT2	1074±10	25.4±0.4	83.35±0.12	1.01	0.0042	no	yes

This is the author's peer reviewed, accepted manuscript. However, the online version of record will be different from this version once it has been copyedited and typeset.

PLEASE CITE THIS ARTICLE AS DOI: 10.1063/1.5115350

645
646

TaC-HT2	1072±10	27.5±0.4	82.95±0.14	1.15	0.0042	no	yes
TaC-HT2	1073±10	29.4±0.4	82.65±0.12	1.12	0.0043	no	yes
TaC-HT2	1075±10	31.5±0.5	82.38±0.12	1.15	0.0043	no	yes
TaC-HT2	1074±10	32.9±0.5	82.04±0.12	1.14	0.0044	no	no
TaC-HT2	1073±10	34.9±0.5	81.78±0.12	1.21	0.0046	no	no
TaC-HT2	1073±10	36.1±0.5	81.52±0.13	1.29	0.0046	no	no
TaC-HT2	1072±10	37.8±0.5	81.28±0.12	1.25	0.0048	no	no
TaC-HT2	1073±10	38.8±0.5	81.09±0.14	1.37	0.0049	no	no

This is the author's peer reviewed, accepted manuscript. However, the online version of record will be different from this version once it has been copyedited and typeset.

PLEASE CITE THIS ARTICLE AS DOI: 10.1063/1.5115350

647

Table III

This study	Parameter	1σ stdev
V_0 (\AA^3)	88.478	0.020
K_{T0} (GPa)	305	5
$(dK_T/dP)_{T0}$	6.1	0.5
γ_{th0}	1.2	0.1
Q	1	2
θ_0 (K)	567	10

648

649

650 Table IV

Reference	Ref.#	Method	Composition	V_0 (\AA^3)	Density (g/cm^3)	K_0 (GPa)	G (GPa)	$(dK/dP)_0$	E (GPa)	Poisson's
This study		A-XRD + R-XRD	TaC _{0.99}	88.478	14.448	305±5		6.1±0.5		
Brown et al. (1966)	[28]	Thin rod Ultrasound resonance	TaC _{0.994}	88.424	14.489	344	216		537	0.24
Bartlett & Smith (1967)	[29]	Ultrasound pulse-echo	TaC _{0.90}		14.65	217±7	120±25		304±64	0.27
Jun & Shaffer (1971)	[30]	Ultrasound resonance	TaC _{0.99}	88.359	14.496	345	216.8		537.7	
Smith & Glaser (1973)	[17]	Neutron Inelastic Scattering	TaC	88.448	14.491	283 ^r	194		474	0.22
Bukatov et al. (1975)	[66]	Ultrasound pulse-echo	TaC _{0.99}			317	227		552	0.21
Dodd et al. (2003)	[31]	Ultrasound pulse-echo	TaC _{0.98}		14.478	332±39	234±27	4.97±0.25	567±68	0.215
Liermann et al. (2005)	[32]	A-XRD (AI PTM)	TaC _{0.98}			340±5		4*		
		A-XRD (nonhydrostatic)	TaC _{0.98}			347±2		4*		
		A-XRD (all data)	TaC _{0.98}			345±9		4±0.4		
López de-la-Torre et al.(2005)	[33]	Ultrasound resonance	TaC		14.64					
		DFT (LDA)	TaC	85.533	14.985	365±4		3.6±0.2		
		DFT (GGA)	TaC	92.652	13.833	318±4	191		550	0.21
Wu et al. (2005)	[34]	DFT (LDA)	TaC	85.184	15.046	357	215		536	0.25
Shanoun et al. (2005)	[16]	DFT (LDA)	TaC	84.605	15.149	397.6	390	3.64	882	0.13
		DFT (GGA)	TaC	89.915	14.254	318.98	313	4.34	708	0.13
Isaev et al. (2007)	[13]	DFT (GGA)	TaC	89.315	14.350	324				
		DFT (GGA)+Debye-Grüneisen	TaC			317	162		514	0.23
Peng et al. (2009)	[36]	DFT (GGA)	TaC	94.756	13.526	311	188	4.32	470	0.248
Li et al. (2011)	[15]	DFT (LDA)	TaC	86.586	14.802	365.3	168.8		438.8	0.3
		DFT (GGA-PBE)	TaC	95.069	13.482	304.9	120.9		320.3	0.32
		DFT (RPBE)	TaC	95.194	13.464	303.1	120.6		319.5	0.32
		DFT (PW91)	TaC	95.256	13.455	302.3	117.6		312.3	0.33
Chen et al. (2013)	[37]	A-XRD	TaC nano	88.478	14.486	433±7		4*		
		DFT (LDA)	TaC	88.478	14.486	371±3	274	4.29	660	0.21
		DFT (GGA)	TaC	88.478	14.486	310±2	221	4.25	537	0.21
Liu et al. (2014)	[38]	DFT (GGA)	TaC	96.072	13.341	293.5	166.4		491.8	0.221
Sai Gautam et al. (2014)	[39]	DFT (GGA-PBE)	TaC	87.884	14.584	344	229		563	0.227
Yu et al. (2014)	[6]	DFT (GGA)	TaC	89.315	14.350	340	214		531	0.24

651

This is the author's peer reviewed, accepted manuscript. However, the online version of record will be different from this version once it has been copyedited and typeset.
PLEASE CITE THIS ARTICLE AS DOI: 10.1063/1.5115550

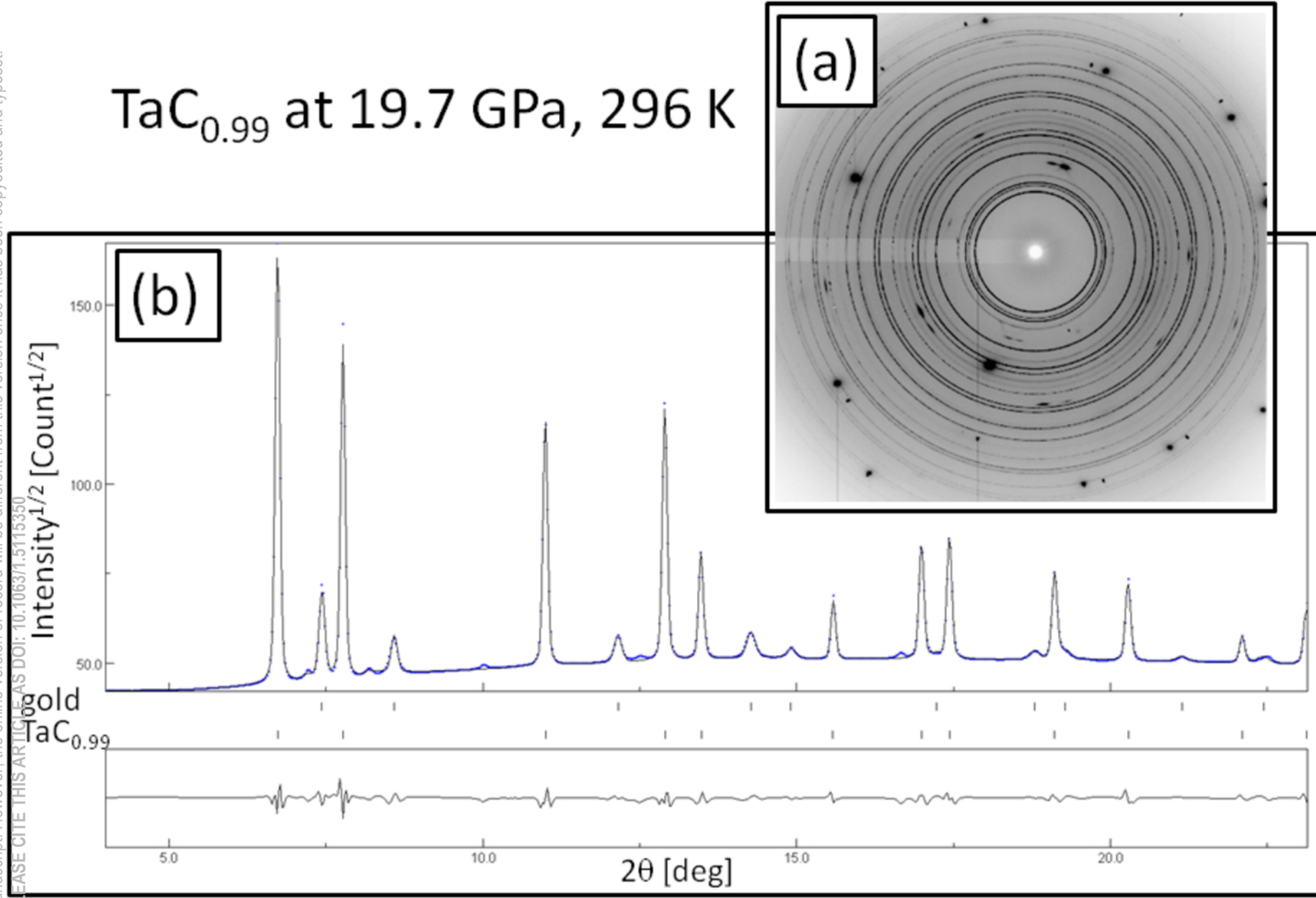
652 Table V

Reference	Ref.#	Method	Composition	Density (g/cm ³)	α_0 (10 ⁻⁶ K ⁻¹)	C_P (JK ⁻¹ Mol ⁻¹)	θ_0 (K)	γ_{th}	V_0 (Å ³)
Houska (1964)	[20]	EXP	TaC _{1.02}	14.538	18				88.270
Kempton (1969)	[19]	EXP	TaC _{0.994}				572		
Kelley (1940)	[21]	EXP	TaC			36.66			
Elliott & Kempton (1958)	[22]	EXP	TaC _{0.984}	14.491	19.77				88.360
Jun & Shaffer (1971)	[23]	EXP	TaC _{0.99}		20.01				
Jun & Shaffer (1971)	[30]	EXP	TaC _{0.99}	14.496			556	1.47	88.360
Dodd et al. (2003)	[31]	EXP	TaC _{0.98}	14.478			593±71		
Lu et al. (2007)	[35]	COMP	TaC				808	2.34	
Peng et al. (2009)	[36]	COMP	TaC	13.526	21		541	2.08	94.760
Liu et al. (2014)	[38]	COMP	TaC	13.341			509.4		96.07
Sai Gautam et al. (2014)	[39]	COMP	TaC	14.584		38.93	588.3		87.883
Frisk & Guillermet (1996)	[24]	COMP	TaC			36.61	551		

653

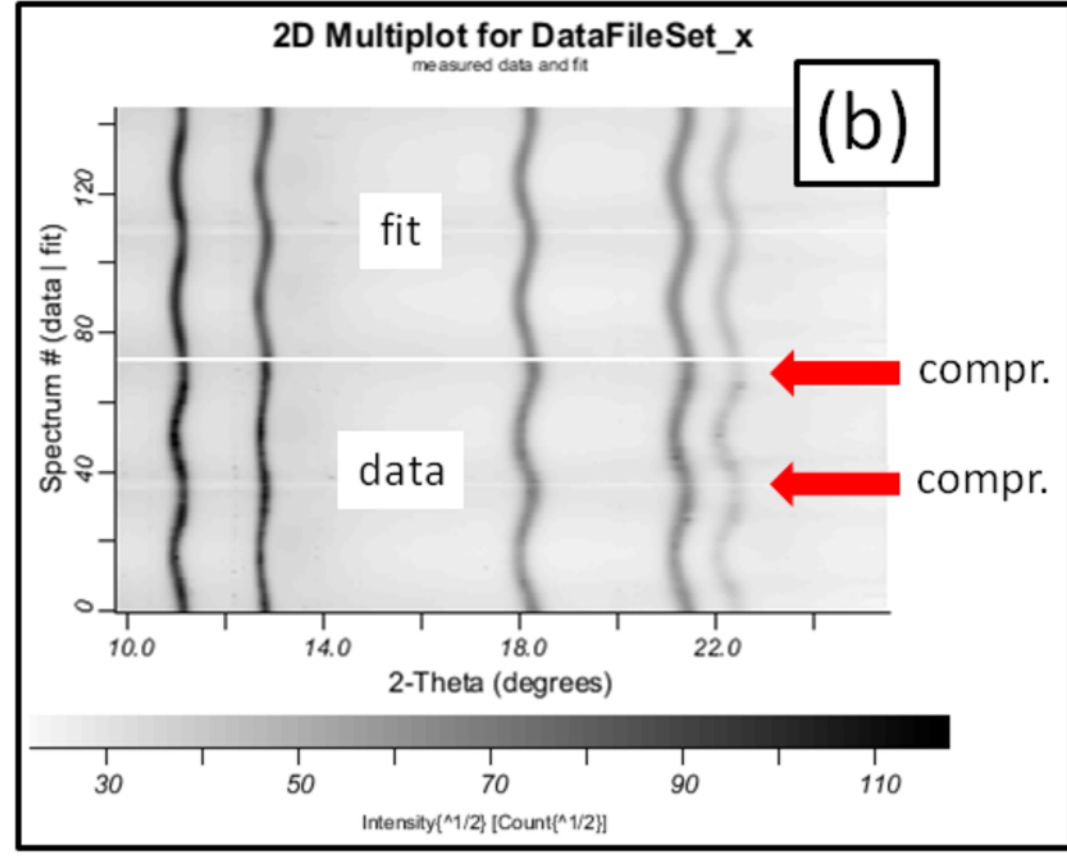
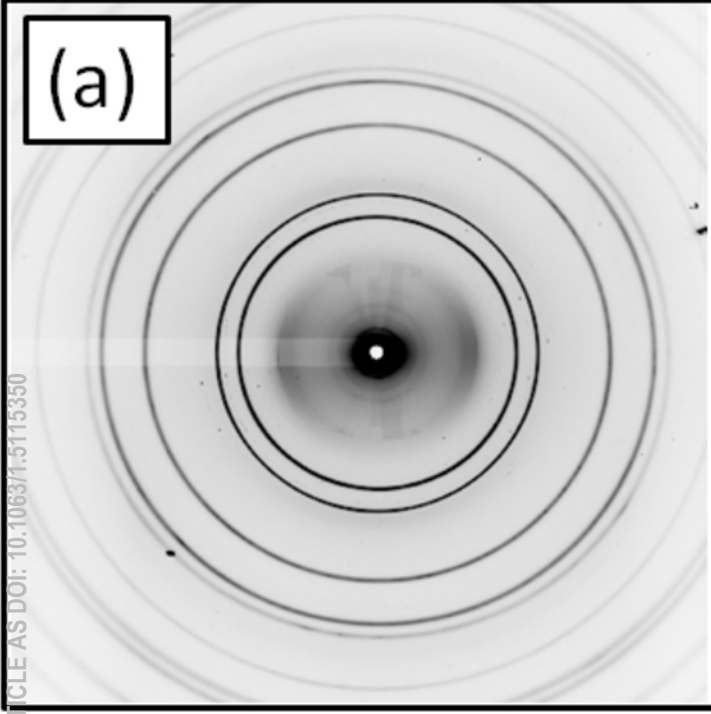
This is the author's peer reviewed, accepted manuscript. However, the online version of record will be different from this version once it has been copyedited and typeset.

PLEASE CITE THIS ARTICLE AS DOI: 10.1063/1.5115350

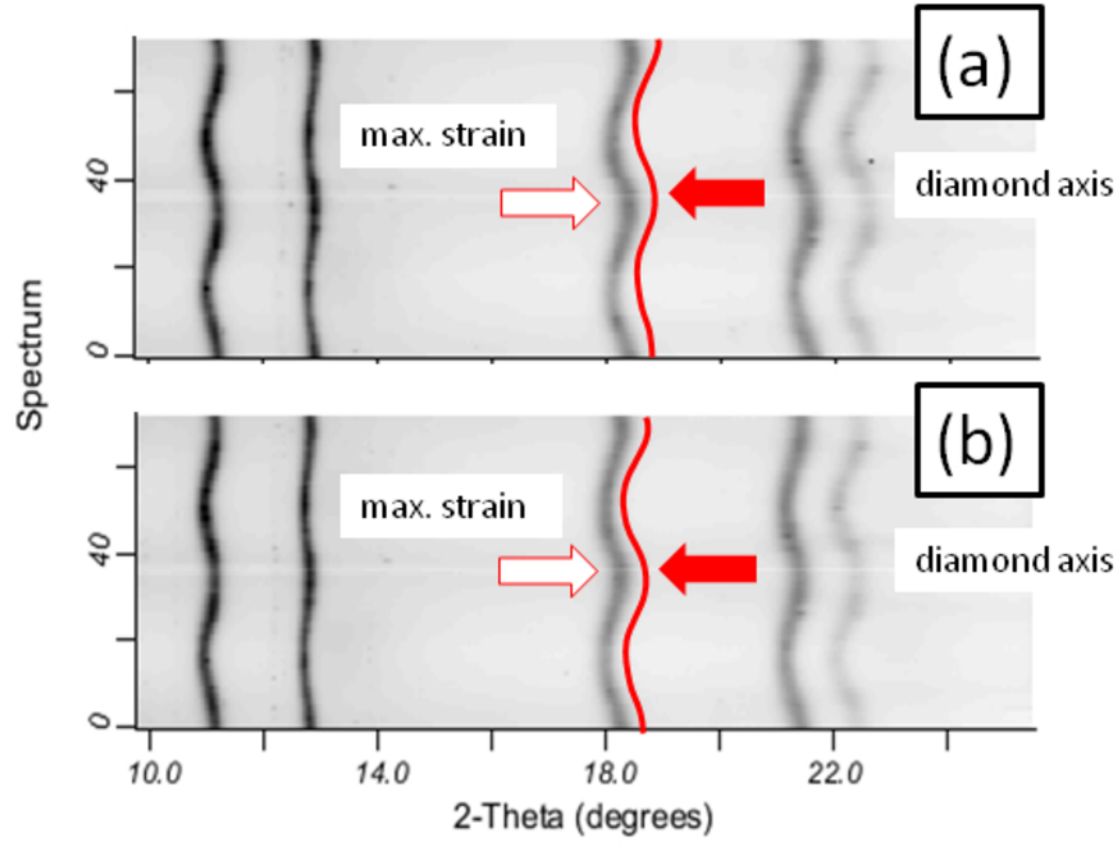


This is the author's peer reviewed, accepted manuscript. However, the online version of record will be different from this version once it has been copyedited and typeset.
PLEASE CITE THIS ARTICLE AS DOI: 10.1063/1.5115350

TaC_{0.99} at 29.4 GPa, 1073 K

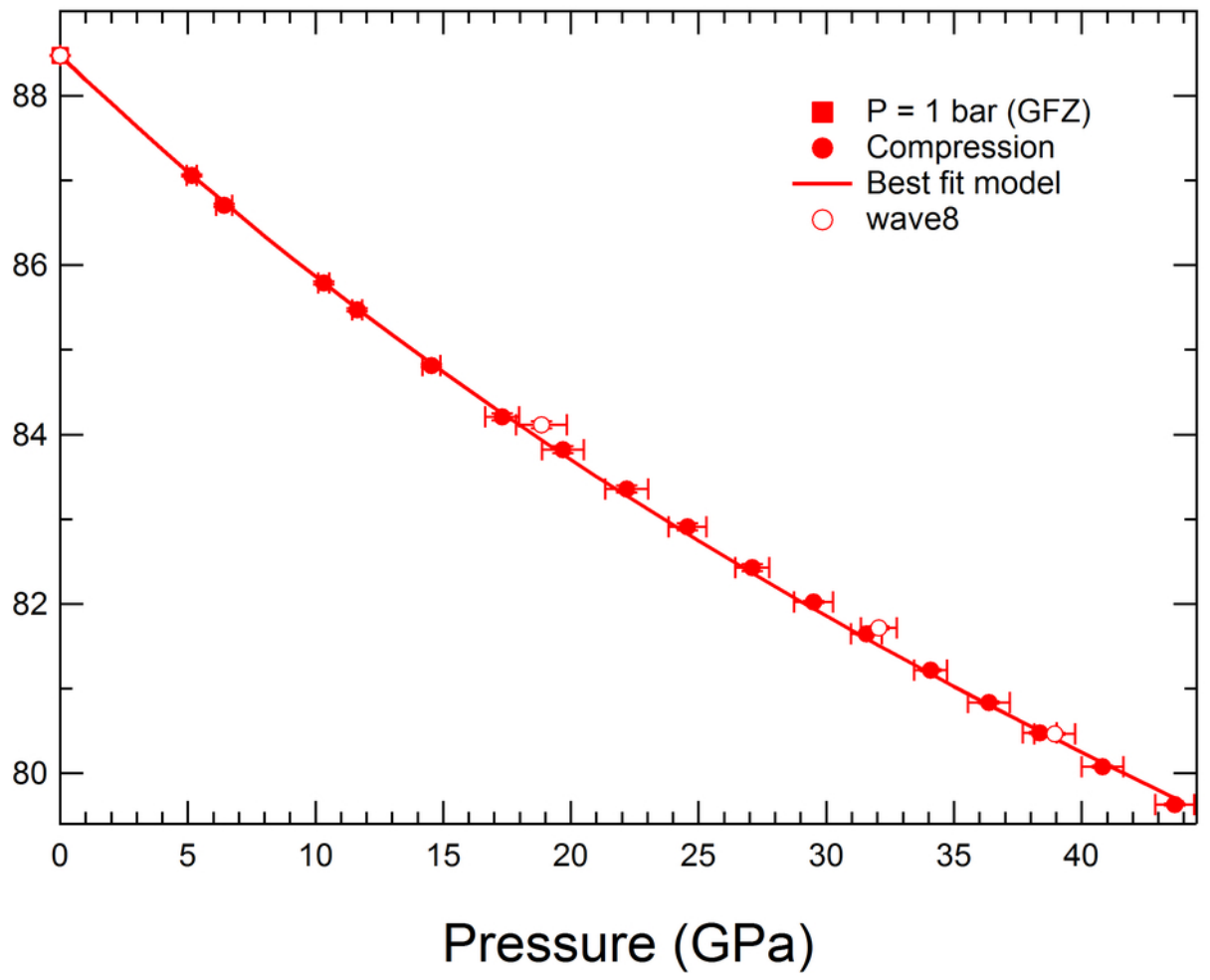


This is the author's peer reviewed, accepted manuscript. However, the online version of record will be different from this version once it has been copyedited and typeset.
PLEASE CITE THIS ARTICLE AS DOI: 10.1063/1.5115350



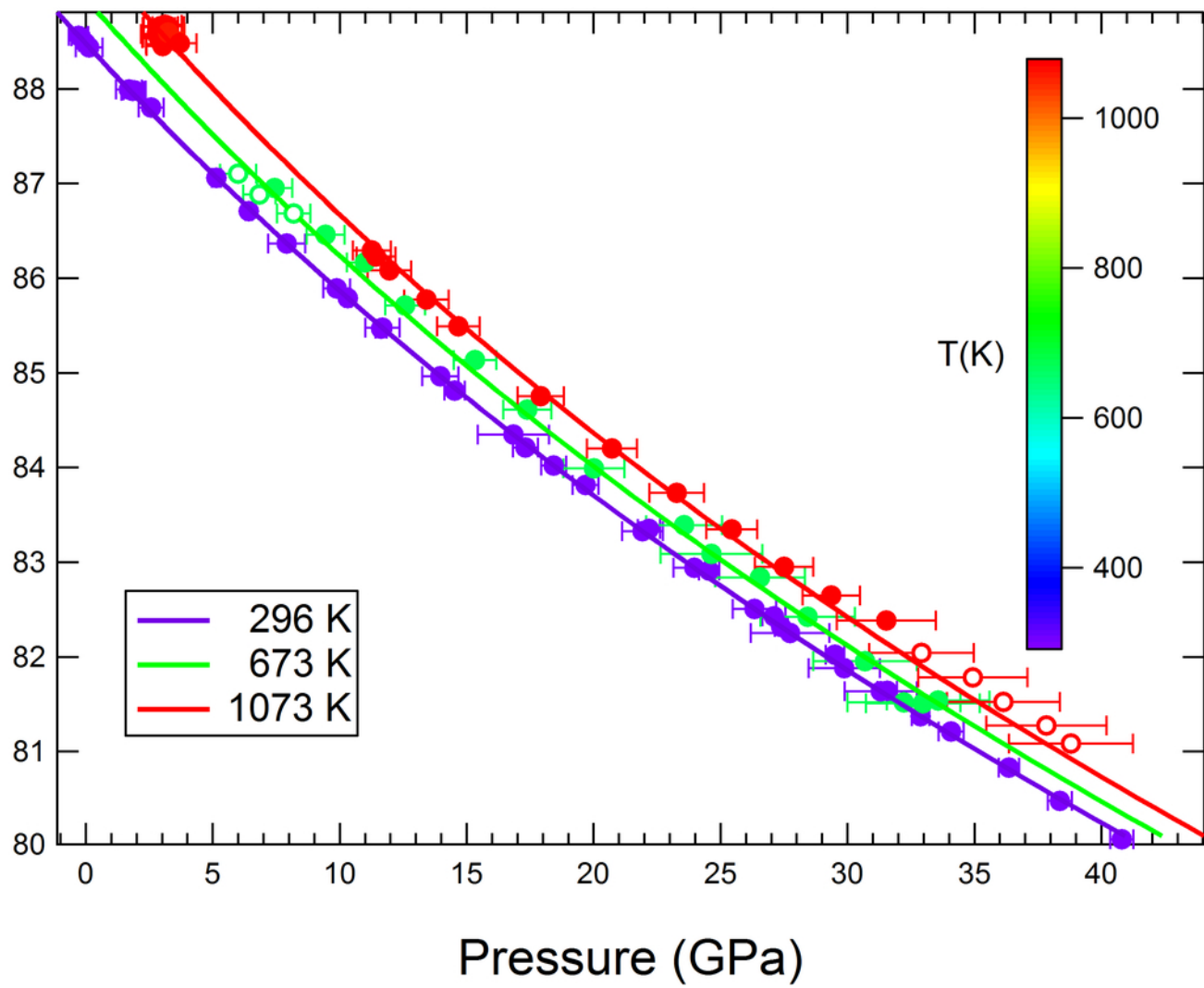
This is the author's peer reviewed, accepted manuscript. However, the online version of record will be different from this version once it has been copyedited and typeset.
PLEASE CITE THIS ARTICLE AS DOI: 10.1063/1.5115350

Unit cell volume (\AA^3)



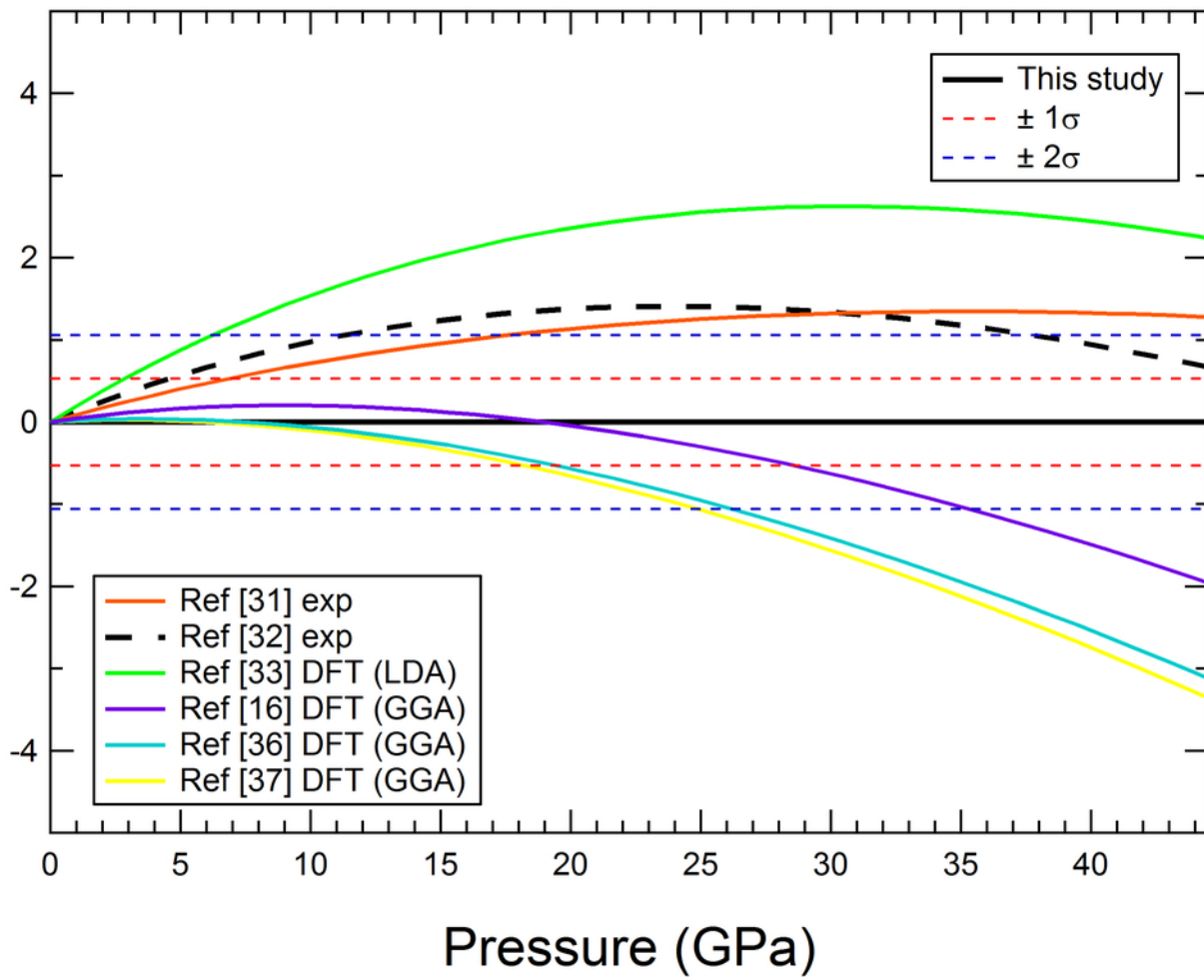
This is the author's peer reviewed, accepted manuscript. However, the online version of record will be different from this version once it has been copyedited and typeset.
PLEASE CITE THIS ARTICLE AS DOI: 10.1063/1.5115350

Unit cell volume (\AA^3)



This is the author's peer reviewed, accepted manuscript. However, the online version of record will be different from this version once it has been copy edited and typeset.
PLEASE CITE THIS ARTICLE AS DOI: 10.1063/1.5115350

P - P this study (GPa)



This is the author's peer reviewed, accepted manuscript. However, the online version of record will be different from this version once it has been copyedited and typeset.
PLEASE CITE THIS ARTICLE AS DOI: 10.1063/1.5115350

Grüneisen parameter γ 